Modeling plasticity of MgO by 2.5D dislocation dynamics simulations

Riccardo Reali, Francesca Boioli, Karine Gouriet, Philippe Carrez, Benoit Devincre, Patrick Cordier

Materials Science & Engineering A 690 (2017) 52–61

Contents lists available at ScienceDirect

Materials Science & Engineering A

journal homepage: www.elsevier.com/locate/msea

Modeling plasticity of MgO by 2.5D dislocation dynamics simulations

Riccardo Reali[a,*], Francesca Boioli[b], Karine Gouriet[a], Philippe Carrez[a], Benoit Devincre[c], Patrick Cordier[a]

[a] Unité Matériaux et Transformations (UMET), University of Lille, CNRS UMR 8207, F-59655 Villeneuve d'Ascq Cedex, France
[b] Institut Lumière Matière (ILM), CNRS UMR 5306, Université Claude Bernard Lyon 1, F-69622 Villeurbanne Cedex, France
[c] Laboratoire d'Etude des Microstructures (LEM), CNRS-ONERA UMR 104, F-92322 Chatillon Cedex, France

ARTICLE INFO

Keywords:
MgO
Periclase
High-temperature plasticity
Creep
2.5D dislocation dynamics

ABSTRACT

In this study, we model the plasticity of MgO (periclase) using a 2.5-dimensional (2.5D) dislocation dynamics (DD) simulation approach. This model allows us to incorporate climb in DD simulations to model the creep behavior at high-temperature. Since a 2D formulation of DD cannot capture some important features of dislocation activity (e.g. those involving line tension), local rules are introduced to take these features into account (this is the 2.5D approach). To ensure the validity of such approach, the model is applied over a wide temperature range with a view in the lower temperature regimes where the newly introduced mechanism (climb) is not active, to benchmark our model against previous 3D simulations and experimental data. Thus we consider successfully a low temperature ($T \leq 600$ K) regime where plasticity is dominated by dislocation glide in the thermally activated regime; an intermediate regime ($T = 1000$ K) where plasticity is dominated by dislocation-dislocation interactions; and a high-temperature regime ($1500 \leq T \leq 1800$ K) which is the actual goal of the present study and where creep plasticity is governed by dislocation glide controlled by recovery (climb being considered here). We show that, taking into account the range of oxygen self-diffusion coefficients available in the literature, our simulations are able to describe properly the high-temperature creep behavior of MgO.

1. Introduction

Periclase (MgO) is a model ceramic which exhibits the rock salt structure. It has been extensively studied for several decades because of its potential uses as a refractory material ($T_f > 3000$ K at ambient pressure). Alloyed with ca. 10% iron, MgO is also the second most abundant phase of the Earth's lower mantle after a magnesium-silicate named bridgmanite. Therefore, the study of MgO plastic properties is of great interest in both geophysics and materials science.

Recently, substantial developments have been achieved to model plasticity based on multiscale numerical modeling with most efforts being devoted to metallic systems. In non metallic solids, most developments have been made on MgO because of the general interest mentioned above and since abundant experimental data are available for benchmarking. Starting from the atomic scale, the individual properties of gliding dislocations have been modeled leading to a satisfactory description of lattice friction and of the critical resolved shear stresses of single crystal MgO as a function of temperature [1] and pressure [2]. Recently, this approach has been extended to the plastic behavior of aggregates under pressure [3]. So far, these models could only take into account dislocation glide. Since the relevance of MgO is mostly related to high-temperature applications or to its creep behavior in the Earth's mantle, a further effort was needed to model creep in MgO at high temperature. In fact, under these conditions dislocation climb is expected to play a significant role during creep deformation and needs to be included in the model.

In this work, we address the influence of climb on MgO plasticity by using 2.5D-DD simulations. Within this method we use a simplified 2D framework and we include local rules to take into account the relevant 3D mechanisms. This allows us to adopt a simple model that can capture the most important 3D dislocation mechanisms and readily include the interplay between glide and climb in the high temperature regime.

We first use the 2.5D-DD method to describe the plasticity of MgO in the low ($T \leq 600$ K) and intermediate ($T = 1000$ K) temperature regimes, where only dislocation glide is active. This allows to benchmark our 2.5D approach against 3D-DD simulations. Furthermore, comparisons with experimental data are also made to show that our 2.5D-DD simulations are able to reproduce the key features of deformation in these two temperature regimes.

* Correspondence to: University of Lille, Unité Matériaux et Transformations (UMET), CNRS UMR 8207, Bat C6, 59655 Villeneuve d'Ascq Cedex, France.
E-mail address: riccardo.reali@ed.univ-lille1.fr (R. Reali).

http://dx.doi.org/10.1016/j.msea.2017.02.092
Received 25 November 2016; Received in revised form 7 February 2017; Accepted 23 February 2017
Available online 24 February 2017
0921-5093/

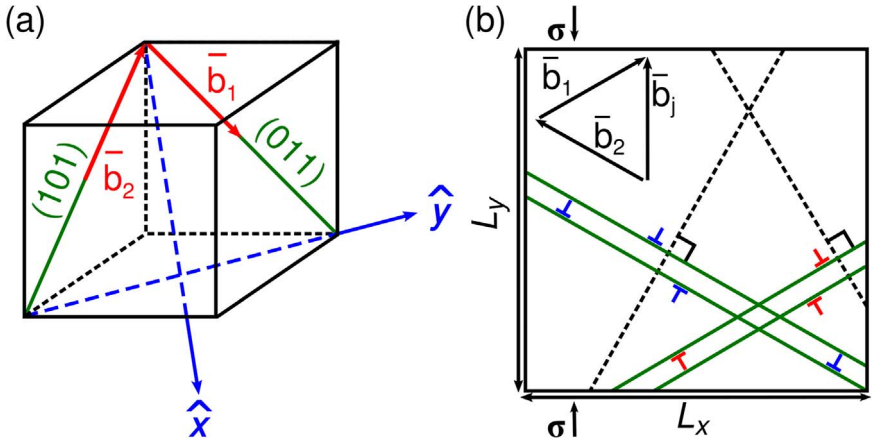

Fig. 1. (a) Representation of the cubic cell of MgO (in black) with the chosen Burgers vectors b_1 and b_2 (red arrows), to which are associated the respective slip planes (green lines). The reference system axes $\hat{x}$ and $\hat{y}$ are identified by the blue arrows. (b) Sketch of the simulation box lying in (111) plane, where dislocations belonging to the two slip systems glide accordingly to the directions of the two Burgers vectors. Junction Burgers vector b_j is also shown. Black, dashed lines show the two climb directions which are perpendicular to the glide planes (identified by green lines). Stress σ is applied along $\hat{y}$ direction. (For interpretation of the references to color in this figure legend, the reader is referred to the web version of this article).

Then we introduce dislocation climb to model creep in the high temperature regime ($1500 \leq T \leq 1800$ K). Our results are compared with data from MgO creep experiments.

2. Method

To model plasticity of periclase we use a 2.5-dimensional (2.5D) dislocation dynamics (DD) simulation approach. DD simulation is a modeling tool which describes the collective motion and interactions of dislocations at the mesoscale. This technique is based on continuum elasticity theory, which provides the description of the elastic field induced by dislocations in a crystal, their interactions with each other and with respect to the stress field resulting from external loading [4].

Although several DD codes have been designed to model different processes and materials, they all share a few key features. First, dislocations are discretized into a finite ensemble of line segments. Then, forces acting on each segment are calculated from elasticity theory and the velocity of each segment is calculated according to a material-dependent equation of motion. The displacements of segments are obtained by integrating velocity with a simple Euler algorithm. Furthermore, DD codes can account for the relevant atomistic processes controlling dislocation mobility and interactions by introducing local rules [5,6]. The treatment of these local rules constitutes the main difference between DD codes.

3D-DD formulations allow describing dislocation lines of edge, screw and mixed characters in a three-dimensional space, accounting for their curvature, topology and interactions. This approach naturally captures the evolution and organization of dislocation lines but it can be complex and computationally demanding. A 2D formulation, where dislocation lines are treated as straight infinite lines, is sometimes sufficient to address some fundamental questions in plasticity. This method reduces the number of degrees of freedom with respect to 3D simulations but makes possible to reach potentially larger amounts of plastic deformation and to take into account dislocation properties difficult to model in 3D. On the other hand, the 2D modeling of dislocation dynamics fails to catch important dislocation properties such as dislocation line tension which controls, for instance, multiplication processes. The latter limitations may be overcome by adopting the so called 2.5D-DD approach, where additional local rules are introduced in the 2D simulation plane in order to mimic as closely as possible important 3D mechanisms, such as dislocation sources or multiplication [7,8]. This type of simulations has been successfully employed, for example, to investigate dislocation patterning [8] or to reproduce the transition between stage I and stage II in fcc metals [9]. In this work, we model dislocation climb by adopting a 2.5D-DD approach, similarly to Davoudi et al. [10], Keralavarma et al. [11] and Boioli et al. [12]. To characterize the dislocation behavior of periclase in a wide range of temperatures, different controlling mechanisms need to be encompassed in the model.

Within our code, dislocation glide is coupled with climb in order to investigate plasticity in the high temperature regime, while at low and intermediate temperatures, which are considered for benchmarking, climb is expected to play a minor role, and only glide is considered. Therefore, in this work, the key simulation inputs are the parameters chosen to characterize glide and climb mobility laws.

Periclase is an ionic face-centered cubic oxide, which exhibits a rock-salt structure of space group $Fm\bar{3}m$ with a lattice parameter a=4.22 Å. The easiest slip systems are ½ < 110 > {110} followed by ½ < 110 > {100}, both having Burgers vector magnitude b=2.99 Å. At ambient pressure, dislocations belonging to the ½ < 110 > {110} family glide at lower stresses than dislocations belonging to the ½ < 110 > {100} family in a wide range of temperatures [13,14]. Therefore, in this study, we focus on dislocations of the easiest slip family – i.e. ½ < 110 > {110} – by including in the code two slip systems belonging to it. The simulation box is a square of size L_x=L_y and dislocation lines are introduced as straight segments of constant length L=1 μm perpendicular to the reference plane. This 2D reference plane in our simulations is (111), where both the considered glide and climb directions lie, as sketched in Fig. 1. The slip systems considered are identified by the Burgers vectors b_1=½ [01$\bar{1}$] and b_2=½ [$\bar{1}$01]. Hence, the dislocation lines are all of edge character and glide in planes (011) and (101), respectively (Fig. 1a). The dislocation climb direction is perpendicular to the glide direction. The reference system chosen for the simulation box has directions $\hat{x}$ = [11$\bar{2}$] and $\hat{y}$ = [$\bar{1}$10]. Stress is applied along the $\hat{y}$ direction in order to symmetrically load the two slip systems, resulting in a Schmid factor equal to 0.433 for both of them. Dislocations gliding in different planes may cross each other and form junctions which are oriented along the direction of intersection between the two planes. Planes of the ½ < 110 > {110} family can intersect each other at 90° or 120° and only in the latter case the sum of the two Burgers vectors is energetically favorable in order to create a junction [14]. The resulting segment has an edge character and can potentially glide in {112} planes, which are not among the reported easy slip planes of periclase. In this study, we consider two glide planes that form an angle of 120°,

Table 1
Parameters inserted in the glide velocity law for dislocation mobility in the thermally activated regime (from [1]).

	½ < 110 > {110}
τ_P (MPa)	150
ΔH_0 (eV)	1.14
p	0.5
q	2.0
l_c (nm)	33.8

allowing for the formation of junctions with Burgers vector $b_3=b_1+b_2=½\,[\bar{1}10]$, having the same orientation as $\hat{y}$ (Fig. 1b).

Isotropic elastic constants for MgO are used: a shear modulus with a temperature dependence $\mu(T)=140\ \text{GPa}-0.0255\times T$ [15] and a Poisson ratio $\nu=0.18$ [16]. Where not otherwise specified, an initial dislocation density $\rho=10^{12}\ \text{m}^{-2}$ is set in the simulations, with a linear simulation frame size $L_x=L_y$ equal to 10 μm.

Laws governing dislocation multiplication and annihilation are included in the 2.5D-DD code to reproduce these fundamental 3D mechanisms, as proposed by Benzerga et al. [9] and Gomez-Garcia et al. [8]. First, a law reproducing the experimental observation that the dislocation density increases linearly with the plastic strain $d\rho/d\varepsilon=m$ is used. Here m is the rate at which the dislocation density increases with the plastic strain, assuming annihilation events not to occur or to be rare. This law describes the expansion of dislocation loops in a 3D volume under the influence of a stress field. In the present work, the constant m is $1\cdot10^{15}\ \text{m}^{-2}$ according to the results of 3D simulations in duplex slip. Furthermore, an annihilation rule is used to reproduce the fact that dislocations forming a dipole (i.e. two dislocations having the same Burgers vector but of opposite sign) can mutually annihilate when they approach each other. The annihilation rule consists in allowing dislocations forming a dipole to annihilate when the height of the dipole (i.e. their distance) is smaller than a critical value given as an input parameter.

These two rules are applied in all three temperature regimes. Nevertheless at low and intermediate temperatures, while multiplication is constantly operating through the motion of dislocation lines, the annihilation events take place less frequently. This is due to the absence of recovery processes, such as climb or cross-slip, that allow dislocations to move from one slip plane to another one, hence promoting dislocation-dislocation annihilation. In fact, these mechanisms are effective only at significant temperatures. As a consequence, in the first two regimes, annihilation events are quite rare, since dislocations cannot move out of their glide planes and the distance between two dislocations forming a dipole is given by the distance between their two slip planes. Thus, the evolution of dislocation density is mostly governed by the multiplication rule and it increases with the applied stress.

On the contrary, when at high temperatures climb is active, dislocations can change their glide plane by climb. Dislocations in a dipole configuration may consequently approach each other till they reach the given critical distance and annihilate. The dislocation density in the third regime is then controlled by the interplay between dislocation multiplication and dislocation annihilation promoted by climb. This leads to a steady-state condition where, with respect to time, the dislocation density fluctuates around an equilibrium value and the deformation increases linearly. These equilibrium values depend on the different stresses applied to the simulation box.

Therefore, at ambient pressure, plastic deformation in MgO is expected to be controlled by several mechanisms depending on the temperature range investigated. These features and the respective modeling approaches will now be presented for the low ($T\leq600$ K), intermediate ($T=1000$ K) and high ($1500\leq T\leq1800$ K) temperature regimes.

3. Results

3.1. Low temperature regime

At low temperature ($T\leq600$ K), dislocation glide dominates and plastic flow is controlled by the relatively low mobility of dislocations. The plastic strain limiting mechanism is then lattice friction which involves a thermally activated kink-pair nucleation process [1]. In this thermally activated regime, the velocity v_g of a dislocation of length L can be described by the mobility law proposed by Kocks et al. [17]:

$$v_g = b\frac{L}{l_c}\nu_D\frac{b}{l_c}exp\left(\frac{-\Delta H(\tau)}{k_BT}\right) \tag{1}$$

where b is the magnitude of the Burgers vector, l_c is the critical width of kink pairs, ν_D is the Debye frequency, k_B is the Boltzmann constant and $\Delta H(\tau)$ is the critical activation enthalpy of kink-pair nucleation as a function of the effective resolved shear stress τ acting on the considered dislocation. The latter quantity, $\tau=\tau_{app}+\tau_{int}$ is calculated at each simulation step for each segment, and it represents the combination of external loading field (τ_{app}) and the internal stress field due to the dislocation microstructure (τ_{int}), both projected along the dislocation glide direction [12]. In particular, the contribution of τ_{int} at one dislocation position is given by the sum of the elastic fields induced by all the dislocations in the microstructure (except the one considered) at such position [4]. T is the temperature.

The kink pair activation enthalpy $\Delta H(\tau)$ in Eq. (1) is formalized in the present study accordingly to Kocks et al. [17]:

$$\Delta H(\tau) = \Delta H_0\left[1-\left(\frac{\tau}{\tau_P}\right)^p\right]^q \tag{2}$$

where ΔH_0 is the critical activation enthalpy at zero stress, p and q are empirical parameters, and τ_P is the Peierls stress. The parameters used for the glide mobility are provided by Amodeo et al. [1] and reported in Table 1. Here it must be noted that the dislocation character considered in the 2.5D-DD simulation frame are of edge type, but the glide mobility law of Eq. (1), which is identified for screw dislocations, is applied to all dislocation characters for simplicity reason.

To model plastic deformation under these conditions, single slip simulations were run at constant laboratory strain rates ($10^{-4}\ \text{s}^{-1}$). Our model is validated through the comparison of the critical resolved shear stresses from our 2.5D-DD simulations with experimental [18–22] and 3D-DD [1] data obtained for MgO in the same range of temperatures and applied strain rates (that is, from 1 to $4.4\cdot10^{-4}\ \text{s}^{-1}$ for all the experimental data displayed). In Fig. 2(a) the stress-strain curves from our model are shown: dislocation motion in this regime is thermally activated and therefore is strongly strain rate dependent. Within practical computation time, plastic yield can be observed at lower stresses only if the temperature is raised. A relation between stress and strain after the yield point could be inferred from our curves, but the relatively small values of hardening coefficient observed in this phase – less than 10^3 MPa as measured by Srinivasan and Stoebe [21] – are difficult to reach without explicitly fitting some input parameters and significantly reducing the initial dislocation density. The evaluation of this feature is thus left to other studies.

In Fig. 2(b) is shown the comparison between the CRSS at different temperatures obtained in the present work and in different numerical and experimental studies on MgO.

3.2. Intermediate temperature regime

At 600 K the athermal threshold temperature T_a is reached for ½ < 110 > {110} slip [1]. Above T_a, lattice friction vanishes and the CRSS does not evolve with temperature anymore. In this athermal regime dislocations move by glide at the free-flight velocity v_{ath} commonly

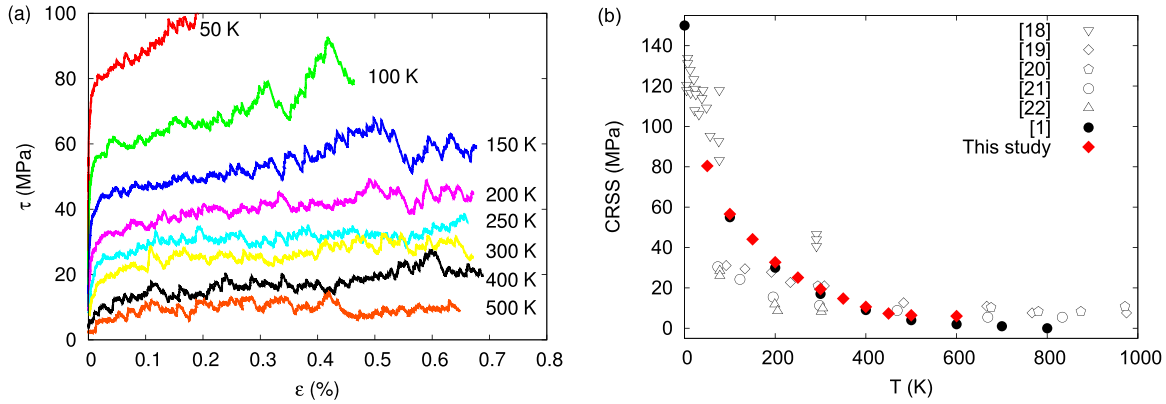

Fig. 2. (a) Resolved shear stress as a function of strain obtained at different temperatures in the thermally activated regime. The threshold value of stress at which plastic flow begins is the critical resolved shear stresses (CRSS). (b) CRSS obtained in this study are compared with results from 3D-DD modeling [1] and other experimental data at different temperatures.

described with a viscous drag equation:

$$v_{ath} = \frac{b\tau}{B} \tag{3}$$

where b and τ were already defined and B is a viscous drag coefficient which varies linearly with temperature [4] and describes the complex interactions between the electric field of a moving dislocation and various elementary excitations, such as conduction electrons and phonons [23]. An experimental measurement of B for MgO is lacking, therefore values between 10^{-4} and 10^{-5} Pa s were assigned for our calculations, depending on the given temperature, knowing that the free-flight mobility law is not expected to play a relevant role in simulations describing plasticity in this regime [16]. In fact, the average velocity of dislocations in the microstructure is limited by their interactions. For this reason, the forest density controls the plastic flow.

Dislocation junction and dipole formation are thought to be the main mechanisms driving strain hardening in fcc crystals. Cross-slip is a possible recovery process but is not included in our 2.5D-DD formulation and the evaluation of its role is left to other studies. However, an earlier numerical experiment on fcc crystals demonstrates that, while cross-slip favors the ordering of dislocation microstructures, it doesn't substantially influence the dislocation density and the stress-strain curves at low strain or low dislocation density [24]. Dislocation interactions and reactions are essentially athermal processes, which can conveniently be treated by elasticity theory. Dipole formation is constitutively taken into account in the code and dislocations forming a dipole are allowed to mutually annihilate when the dipole height is smaller than a critical distance r_a=25b. The latter distance is a fitted value accounting for all possible annihilation reactions that may exist in 3D dislocation dynamics. Reproducing junction formation and destruction in 2.5D is a delicate task since this reaction heavily affects the macroscopic average behavior of the structure. A junction is formed when two attractive dislocations gliding in different planes come to a distance smaller than the average length of junctions under stress, which is estimated from 3D simulations [25]. When this happens, dislocations positions are blocked and the interaction stress between them is set to zero. Once a junction is created, the stress acting on it will be evaluated at each step in the same way described for single dislocations in the paragraph above. The junction will remain stable as long as the stress on each dislocation composing it is lower than a critical value τ_j. If this value is exceeded, the dislocations composing the junction will be unblocked and made free to move. In other words, τ_j represents the critical stress needed to break a junction. The local rule used in the DD code to break a junction is the following: when the stress (i.e. the sum of τ_{app} and τ_{int}) at the junction position reaches the critical value τ_j, the junction is broken. This value is formalized by Gómez-García et al. [8]:

$$\tau_j = \beta \frac{\mu b}{\rho_l^{-1/2}} ln\left(\frac{\rho_l^{-1/2}}{b}\right) \tag{4}$$

where ρ_l is the local density, that accounts for the local spatial heterogeneities in the dislocation density, and β is a constant that is set as an input parameter to recover reasonable values of the strength necessary to destruct the junctions, which in turn affects the flow stress. ρ_l is used here to estimate the length of the junction arm which drives the formation (destruction) of the junction through a zipping (unzipping) mechanism [8]. A value of β=0.035 is usually assigned for fcc metals. In this study, the influence of β on the mesoscopic plastic flow was investigated, running different sets of simulations having the same the initial configuration and β values of 0.02, 0.05 and 0.1.

In the athermal regime, forest interactions are expected to control the plastic flow, leading to the commonly observed dislocation strengthening in fcc crystals. To characterize this type of behavior, the relation between flow stress and dislocation density must be investigated. A dislocation strengthening relation, having the form of the Taylor equation, is usually considered to estimate the macroscopic strength resulting from all possible local configurations in the microstructure:

$$\tau_f = \alpha \mu b \sqrt{\rho} \tag{5}$$

where α is a strengthening coefficient, ρ is taken as the total dislocation density and τ_f is the effective average critical stress for all type of obstacles – i.e. the athermal stress required to overcome the forest dislocation network [16]. τ_f can be extracted from our DD simulations and it represents the stress acting on the microstructure in order to maintain constant the applied strain rate. This stress depends on the dislocation density: the higher the latter, the higher will be the stress applied to achieve the same deformation rate. In fact, as we mentioned above, in this regime the recovery mechanisms are not efficient, therefore a high dislocation density raises the number of forest obstacles which in turn prevent the mobile dislocation segments from further displacements. Therefore, τ_f and the corresponding value of the dislocation density ρ are extracted from each simulation and plotted in order to estimate α, that provides an evaluation of the strength of the microstructure.

Simulations in this regime were run at T=1000 K, in the duplex slip mode, and under a constant strain rate of 10^{-1} s^{-1}. Different initial dislocation densities were set equal to $1{\cdot}10^{11}$, $1{\cdot}10^{12}$, $5{\cdot}10^{12}$ and $1{\cdot}10^{13}$ m^{-2}, in order to encompass a broad range of values for the estimation of α, which was then compared with results from experiments on fcc crystals and 3D-DD data obtained for MgO. In fact, DD simulations do not reach large plastic strain amounts, not allowing large increases in dislocation density either. Therefore, simulations starting with different initial dislocation densities are run to test forest strengthening at different virtual levels of strain [22]. No specific rules

are provided for the estimation of the average strength and corresponding dislocation density [23], therefore in this study the protocol defined by Amodeo et al. [16] was employed, in order to better compare the data obtained: stress and dislocation density measurements are done after yield point, at relatively low plastic strains, as soon as the imposed strain rate is reached.

At 1000 K (around 0.3 T_m) the junction formation and destruction mechanisms drive the deformation behavior of MgO. These mechanisms require very high energies, which cannot be provided by thermal fluctuations, and therefore are considered to be essentially elastic and athermal processes [23]. Junction unzipping is the main softening mechanism considered in this regime, since it allows dislocations previously locked in a sessile junction to move and induce further plastic deformation. This process is introduced in the code through the scaling law showed in Eq. (4), where β is a dimensionless measure of the strength of a specific junction configuration. Varying the value of β will change the effective stress necessary to destroy junctions (i.e. τ_j), influencing the average stress acting on the microstructure (i.e. τ_f) in order to maintain the constant applied strain rate. τ_f and therefore α depend on the choice of β. Here we test different values for β in our 2.5D DD simulations to verify for which values we recover the flow stress and the alpha values obtained by both full 3D DD simulations results and experimental data. This can be seen in Fig. 3(a), where simulations run in the same initial configuration with distinct values of parameter β result in different stress-strain curves. The initial dislocation density is $1{\cdot}10^{13}$ m^{-2} for each simulation displayed. The value of junction strength influences the average stress levels of plastic flow in the microstructure, while the dislocation density, due to the multiplication rule described above, remains comparable for all the three curves. In fact, in Eq. (5), ρ is taken as the total density, that is, twice the density of intersecting obstacles seen by each slip system during duplex slip. This process drives the evolution of stress as function of dislocation density, leading to the different α coefficients we found for the strengthening relation, which are shown in Fig. 3(b)–(d). For the three values of β tested – i.e. 0.02, 0.05 and 0.1 – the recovered values of α are 0.21 ± 0.02, 0.26 ± 0.02 and 0.37 ± 0.03, respectively.

3.3. High temperature regime

The forest mechanism described above leads to a progressive increase of the resistance offered by the microstructure to dislocation motion, due to the increase of dislocation-dislocation interactions and dislocation density with plastic strain. In the absence of a recovery mechanism, this process leads to the afore-mentioned work hardening behavior under constant strain-rate loading or to a saturation of strain under constant load (creep mode). At temperatures high enough – i.e. around 0.5 T_m – diffusion becomes an important phenomenon for MgO plasticity, since it favors dislocation climb, a dislocation motion which involves the exchange of matter through the adsorption or emission of point defects on segments having edge character. Dislocation climb outside its initial glide plane helps a dislocation to bypass obstacles and eventually promote dislocation annihilation, making climb an efficient recovery mechanism. Eventually, the combination of glide and climb motions leads to a steady-state regime, where dislocation multiplication and annihilation compensate each other and dislocation density does not increase anymore with strain. In this study we model climb coupled with glide in MgO and we calculate the steady-state creep strain rates. Our results are only compared with experimental data since this regime has not been modeled yet. Creep simulations were performed in double slip conditions, at temperatures from 1500 to 1800 K and constant applied stresses from 30 to 80 MPa.

Dislocation climb is implemented in the code as described by Boioli et al. [12]. Since climb motion is limited by diffusion, some insights on this process in MgO are required, in order to consider the proper input parameters for the proposed mobility law.

During the past decades, diffusion in periclase has been addressed

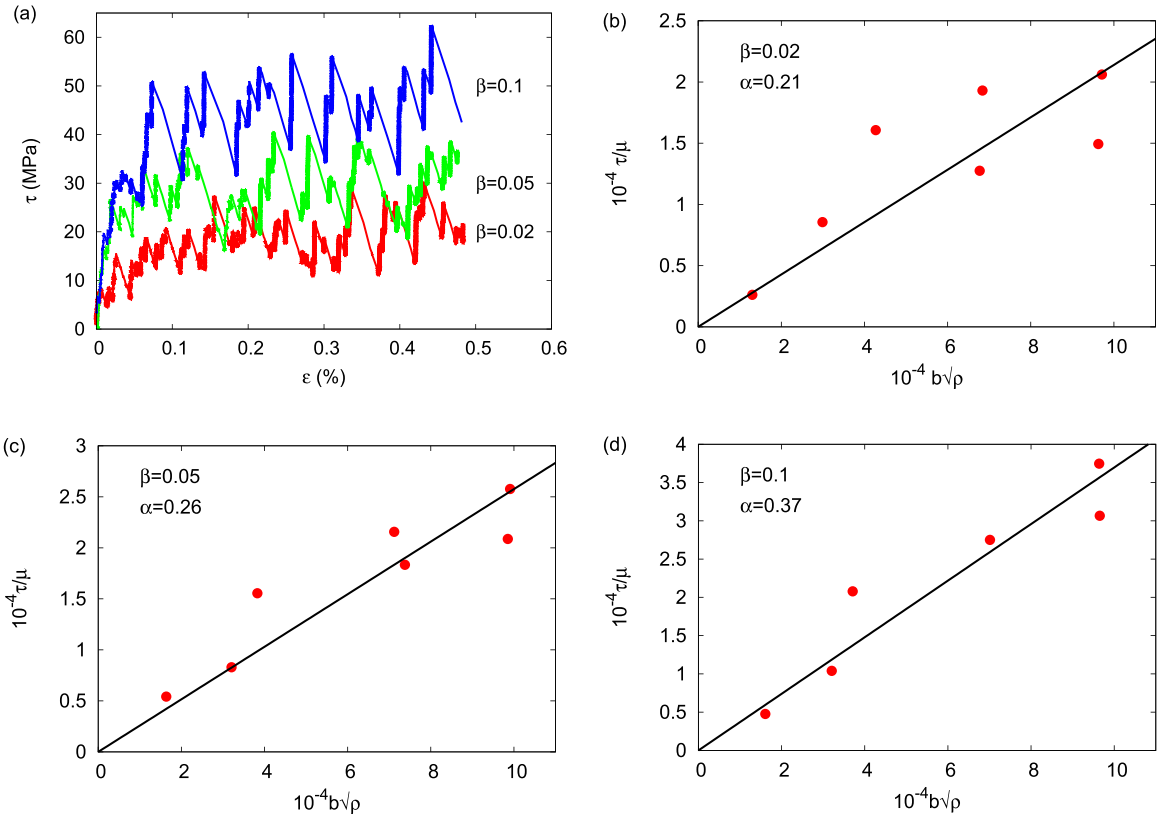

Fig. 3. (a) Stress as a function of strain for three simulations having same initial settings and different values of junctions' strength (β). Initial dislocation density is $1{\cdot}10^{13}$ m^{-2}. (b), (c) and (d) show the different evolution of flow stress as a function of dislocation density, identified by α coefficient, obtained varying the junctions' strength parameter β.

Table 2
Experimental values of self-diffusion pre-exponential factor (D_0) and activation enthalpy (ΔH^{sd}) to compute oxygen self-diffusion coefficient D_{Ox}^{sd}. The main body of simulations was run using the value provided by Yoo et al. [30] while a test was made using also the others at 1700 K [31,32], for which the calculated numerical values of D_{Ox}^{sd} are also shown. Data of Yang and Flynn [32] are shown for both the high and low temperature regimes and only the latter values are employed in the model.

D_0 (m^2/s)	ΔH^{sd} (eV)	T Range (K)	D_{Ox}^{sd} (m^2/s) at 1700 K	References
$2.5\cdot10^{-10}$	2.71	1570–2020	$2.7\cdot10^{-18}$	[31]
$1.8\cdot10^{-10}$	3.24	1270–1920	$5.2\cdot10^{-20}$	[30]
$1.0\cdot10^{-14}$	2.66	1450–1700	$1.5\cdot10^{-22}$	[32]
$7.6\cdot10^{-3}$	6.91	1700–2400		

both experimentally and theoretically. The latter approach suggests that interstitial magnesium and oxygen in periclase are energetically unfavorable: Hirsh and Shankland [26] and references therein suggest enthalpies of 12.4 and 15.2 eV for Frenkel defect formation, for Mg and O respectively. Being these enthalpies rather high, interstitials concentrations in periclase are expected to be very low at equilibrium. Alfè and Gillian [27], through Monte Carlo calculations, find values of formation enthalpy for Schottky defect in periclase around 6.7 eV, almost half of the required energy to create a Frenkel defect. Vacancy mechanism is thus expected to be dominant in periclase diffusion. Diffusion of oxygen may also be assisted by the divacancy defect, which consists in the pairing of a cationic vacancy with an oxygen vacancy [28]. Therefore, while defining the activation volume for diffusion, the formation of both anionic and cationic vacancies will be considered.

Van Orman and Crispin [29] calculated the equilibrium concentration of intrinsic vacancies having a formation energy of 6.7 eV (the Schottky pair free energy of formation) and found out that the equilibrium concentration would be a few ppm at any temperature up to the melting point. It is thus likely that vacancy formation is controlled by extrinsic impurities, most notably the aliovalent, positively-charged, solutes like Fe^{3+}, Al^{3+} and Cr^{3+}. These trivalent species are contained also in ultra-high purity MgO crystals and tend to be present at higher concentrations than monovalent substitutional cations in normal crystals. Extrinsic vacancies will thus mainly have cationic character, with the concentration of extrinsic anion vacancies depending on the inverse of cationic impurities concentration. Therefore, in periclase, while it can be stated that extrinsic cationic vacancies control the Mg self-diffusion at any temperature (also in high-purity crystals) up to the melting point, the same thing is not likely to happen for oxygen vacancies with respect to oxygen self-diffusion. For this reason and also due to the larger ionic radius of oxygen compared to magnesium, oxygen self-diffusion coefficients D_{Ox}^{sd} are 2 or 3 orders of magnitude smaller than those of magnesium at any investigated temperature ([29] and references therein). This implies that absorption or emission of a full MgO unit by a dislocation line is limited by the oxygen vacancy migration and formation processes, since the enthalpy required to form and migrate an oxygen vacancy is much higher than the one required for magnesium. Oxygen self-diffusion is thus the rate-limiting mechanism of diffusion in periclase and will be considered in what follows as the controlling factor on dislocation climb as well.

Thus, for the implementation of diffusion in the climb mobility, the value of the self-diffusion coefficient D^{sd} is taken equal to the oxygen-self diffusion coefficient D_{Ox}^{sd}. This coefficient is expressed with the Arrhenius-type formula:

$$D^{sd} = D_{Ox}^{sd} = D_0 exp\left(\frac{-\Delta H^{sd}}{k_B T}\right) \tag{6}$$

where D_0 is a pre-exponential factor and ΔH^{sd} is the activation enthalpy for oxygen self-diffusion that accounts for point defects formation and migration enthalpy. Here the two parameters D_0 and ΔH^{sd} are taken from experimental data. As we can see from Eq. (6), diffusion is a thermally activated process: this explains why dislocation climb motion, which is directly linked to the diffusion of point defects (Eqs. (6) and (7)), plays an important role in the high temperature regime. At the same time, this process is negligible at low temperatures, where diffusion is extremely slow, and therefore does not contribute significantly to the deformation behavior. The diffusion coefficient of oxygen has been measured experimentally in a wide range of temperatures and sample compositions. Van Orman and Crispin [29] provide a plot which summarizes most of the experimental data on oxygen diffusion in periclase at ambient pressure. Experimental values of the diffusion coefficients display an important variability, embracing up to five orders of magnitude in the temperature range investigated experimentally, which spans from 1100 to 2500 K.

In this study we choose to run the main body of creep simulations using the oxygen self-diffusion coefficient measured by Yoo et al. [30], which provides a single linear fit for a wide range of temperatures. Also, their values fall roughly in the middle of the variability range of experimental measurements. To evaluate the influence of D_{Ox}^{sd} on the simulated creep strain rates, tests were made using also the extreme experimental values measured so far. The parameters and temperature ranges in which they were obtained are shown in Table 2. Oishi and Kingery [31] provide the upper bound value, using samples containing impurities. The inferred mechanism driving oxygen diffusion was assumed to be impurity-controlled or a structure-sensitive process, with the activation energy corresponding to ion mobility. On the other end, Yang and Flynn [32] measured diffusion coefficients on MgO crystals having an ultra-high degree of purity and obtained the smallest values of oxygen self-diffusion coefficients ever observed experimentally. At high temperatures they find an activation energy of 6.9 eV for oxygen diffusion, a value consistent with the activation enthalpy for intrinsic diffusion. However, at lower temperatures, diffusion becomes less activated with a slope resembling that of other studies, with an activation energy of 2.66 eV. This latter value has been chosen, since the range of temperatures investigated in this study falls within this deviation from intrinsic behavior. The temperature at which the data gathered from these studies overlap is around 1700 K, therefore this value was set for simulations addressing the variability of creep strain rates with respect to the chosen oxygen self-diffusion coefficient, D_{Ox}^{sd}. These variations on the creep strain rates are displayed and results are put in perspective with respect to creep data obtained in experiments.

Assuming steady-state conditions, the flux of vacancies from and to the dislocation line is calculated by solving the diffusion equation showed in Eq. (6), allowing for the analytical expression of climb velocity [4,33]:

$$v_c = \eta \frac{D_{Ox}^{sd}}{b}\left[exp\left(\frac{\tau_c \Omega}{k_B T}\right) - \frac{c_\infty}{c_0}\right] \tag{7}$$

where D_{Ox}^{sd} is the oxygen self-diffusion coefficient described above and η is a geometrical factor which depends on the geometry of the flux field. Ω=18.7 Å^3 is the activation volume for self-diffusion, which is here considered to be equal to the formation volume of Mg and O vacancies and is calculated from the unit cell volume of periclase – i.e. $\Omega=a^3/Z$ where Z=4 is the number of formula units per unit cell. τ_c is the effective stress resolved in the climb direction, that is, perpendicular to the glide directions of the two simulated slip systems and is taken positive (negative) if it favors vacancy emission (adsorption). c_∞ is the vacancy concentration far from the dislocation lines (i.e. far from the sources and sinks of vacancies) and c_0 is the intrinsic equilibrium vacancy concentration at a given temperature; $c_0=exp(\Delta H_f/k_B T)$, where ΔH_f is the intrinsic vacancy formation enthalpy. We assume that far from the dislocations, the vacancy concentration is constant and equal to the intrinsic equilibrium concentration – i.e. $c_\infty=c_0$ [12,34]. It is also assumed that the dislocation line is saturated with jogs. The latter assumption implies a cylindrical flux around the dislocation, identified by $\eta = 2\pi/ln\left(\frac{R}{r_c}\right)$ where R and r_c represent the two radii of the cylindrical

surfaces through which the vacancy flux is calculated. r_c is the core radius and R is taken as a fraction of the average dislocation distance. Being within the logarithmic term, the R/r_c ratio does not significantly affect the climb velocity values and here is taken constant and equal to 100 [12,34].

Creep simulations were run to model plasticity of MgO at high temperatures (over 0.5 T_m), where motion by climb is included. Dislocation glide and climb occur on very different time scales, especially in the athermal regime. This difference is accounted in the code by considering two different time steps, with a scheme close to the one proposed by Keralavarma et al. [11]. First, the creep stress is applied to the structure and all the glide events are resolved using the small glide time step, during which plastic strain $\Delta\varepsilon$ is evaluated. Once the configuration in the microstructure gets to a quasi-equilibrium or "jammed" state, dislocations do not glide anymore and the strain saturates. At this point, climb motion is allowed by applying to dislocations the mobility law described in Eq. (7) and by integrating it through the longer climb time step. Once a displacement of a full Burgers vector is reached by climb, the mobility is switched back to glide again and the procedure is repeated iteratively throughout all the simulation.

Creep results at 1600 K are shown in Fig. 4. Fig. 4(a) displays the strain vs time curves obtained from simulations run with (red curve), and without (green curve), including climb motion. After the initial transient stage, glide alone is not capable of producing further deformation: in fact, once the quasi-equilibrium condition is reached, dislocations are trapped into local minimum energy configurations and do not glide anymore under the applied stress (which is constant). In Fig. 4(b) are shown the strain contributions in a creep simulation where both glide and climb are included. The strain produced by dislocations moving in their glide plane (blue curve) is significantly larger than the strain produced by dislocations moving outside their glide plane (green curve). The total strain as a function of time is also shown (red curve, same as the one in Fig. 4a). It is noted, therefore, that even if climb is included, strain is mostly due to dislocations moving by glide. Climb allows dislocations to escape from their glide planes and to be released from "jammed" configurations to eventually bypass obstacles or annihilate. The dislocation microstructure is therefore relaxed and other dislocations are free to move by glide until a new "jammed" state is reached. The repetition of this process leads to the steady-state creep regime, characterized by a constant deformation rate for a given load. This is verified by the linear increase of strain with time that can be observed from the red curves of Fig. 4(a) and (b).

Fig. 5(a) demonstrates that the steady-state condition is observed for different values of applied stress, with strain varying linearly with respect to time for all the curves obtained. The steady-state condition is confirmed also from the evolution of the dislocation density with time, shown in Fig. 5(b), where, after the initial transient, the density fluctuates around a constant value. At a given temperature, the equilibrium density values increase with increasing stress, since the higher the latter, the easier it is to unzip the junctions. These observations confirm that multiplication and annihilation are acting simultaneously during simulations, counterbalancing each other. The former mechanism is related to strain production, which in turn results to be originated by glide motion (Fig. 4b); while the latter is triggered by dislocation getting untangled by climb to other planes to further interact and eventually annihilate.

This study shows that the interplay of glide and climb mechanisms leads to the steady-state creep behavior observed in experiments.

The steady-state creep strain rates depend exponentially on the temperature, therefore the following Arrhenius-type equation is commonly used to describe high temperature deformation:

$$\dot{\varepsilon} = \dot{\varepsilon}_0 \sigma^n exp\left(-\frac{Q}{k_B T}\right) \tag{8}$$

where Q is the activation enthalpy for creep and σ is the applied stress. Q, n and $\dot{\varepsilon}_0$ are generally assumed to be constant and to depend on the mechanism controlling the plastic creep behavior. For MgO, variables like substitutional iron content and oxygen partial pressure seem to have no influence on the power law creep [35].

Our creep results are presented in Fig. 6. The investigated temperatures span from 1500 to 1800 K and the applied creep stresses from 30 to 80 MPa. Fig. 6(a) shows the creep strain rates obtained from the 2.5D-DD simulations as a function of the creep stress, for all tested temperatures. A constant slope is found for these strain rate-stress curves at any temperature. The derivative of the logarithm of creep strain rate with respect to the logarithm of creep stress gives the value of the power law stress exponent, n. All the measurements of n fall within the respective errors with an overall average value of 2.9 ± 0.2. Fig. 6(b) shows the creep strain rates as a function of the reciprocal temperature, for all the tested creep stresses. The activation enthalpy for creep Q can be obtained from the slope of the derivative of strain rate logarithm with respect to the reciprocal temperature T. We obtain a constant value of 3.1 ± 0.2 eV for Q.

Knowing the values of n and Q it is possible to fit also the third parameter of the power law, $\dot{\varepsilon}_0$, obtaining a value of 0.019 ± 0.001 s^{-1}. In Fig. 7 our data are presented together with the respective power law equations, which are plotted using the three averaged parameters at different temperatures.

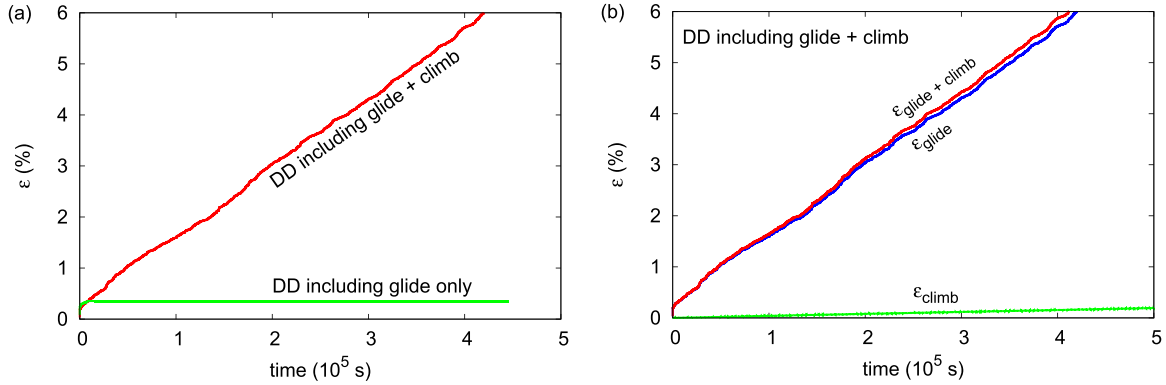

Fig. 4. (a) Strain as a function of time for two simulations run at 1600 K with constant applied load of 60 MPa with (red curve) and without (green curve) including climb mechanism. (b) red curve: total strain as a function of time, same of red curve of (a), where both glide and climb are included. $\varepsilon_{glide+climb}$ is compared with its components due to dislocation glide (ε_{glide}, blue curve) and climb (ε_{climb}, green curve). (For interpretation of the references to color in this figure legend, the reader is referred to the web version of this article).

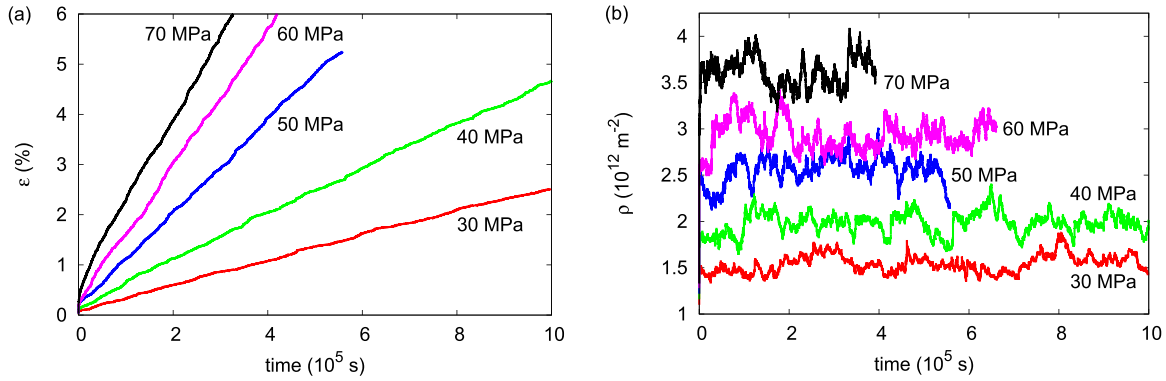

Fig. 5. (a) Strain as a function of time for simulations at 1600 K with applied loads from 30 to 70 MPa. Steady-state condition is reached. (b) Dislocation density as a function of time for the same curves of (a).

Our numerical approach is capable of describing plasticity of MgO at high temperatures, since the relevant mechanisms acting during creep deformation are now included in this formulation.

4. Discussion

In the thermally activated regime, the agreement between the CRSS values obtained from our model and previous data is remarkable (Fig. 2b), especially with the 3D-DD outputs of Amodeo et al. [1]. The comparison with experiments is somehow more complex, since trivalent impurities can interfere with the gliding dislocations, while the modeled motion relies on the overcoming of lattice friction alone. Therefore, for a better comparison, we select experimental data obtained from samples having low impurity contents or being heat treated before analysis [18–22] in order to avoid the impurity-related strengthening effect.

The strengthening coefficients obtained in this study from simulations at 1000 K – i.e. α=0.21, 0.26 and 0.37 – need to be compared with available experimental and numerical data. In the adopted 2.5D-DD framework, according to Gómez-García et al. [8], $\alpha \approx 0.25$. The intermediate value is in fair agreement also with the result of α=0.24 obtained by Amodeo et al. [16] from 3D-DD simulations on MgO for the ½<110>{110} family. The most reliable estimate from DD simulations on fcc crystals, on the other hand, yields $\alpha \approx 0.35$ for a reference forest density of 10^{12} m^{-2} [24]. Basinski and Basinski [36] show that in fcc crystals α varies from 0.5 at lowest densities to about 0.2 for the highest ones, the densities varying from 10^{10} to 10^{14} m^{-2}. Amodeo et al. [16] explain this difference between values of α for MgO and other fcc crystals by either a lack of collinear annihilations, an important ingredient in fcc metals' forest strengthening, or to be due to the higher number of slip systems per family in fcc (12 instead of 6 in MgO). Despite small deviation from the α value found in 3D-DD simulations [16], an overall agreement between the recovered α values and the data available in literature is found. In the athermal regime, plasticity of MgO is controlled by a forest mechanism, as it is commonly observed in fcc metals. We notice that this behavior is significantly different from other mantle phases, for which a significantly larger lattice friction is envisaged at comparable temperatures, resulting in considerably higher stresses to obtain plastic deformation [37–40].

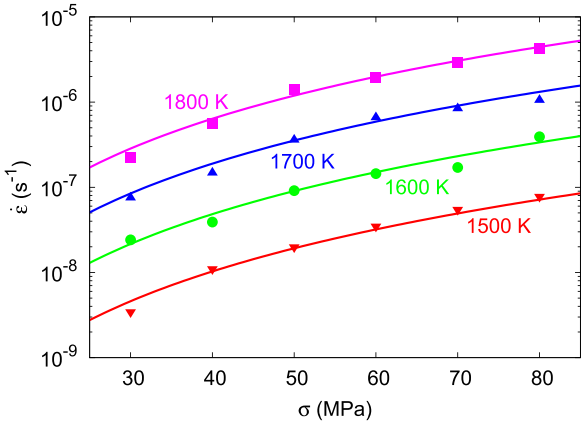

Fig. 7. Creep strain rates as a function of applied stress. Color lines represent the power law curves plotted for the different temperatures using the power law parameters obtained from previous fittings. (For interpretation of the references to color in this figure legend, the reader is referred to the web version of this article).

The results obtained in the low and intermediate temperature regimes prove that the 2.5D-DD approach is suitable to model

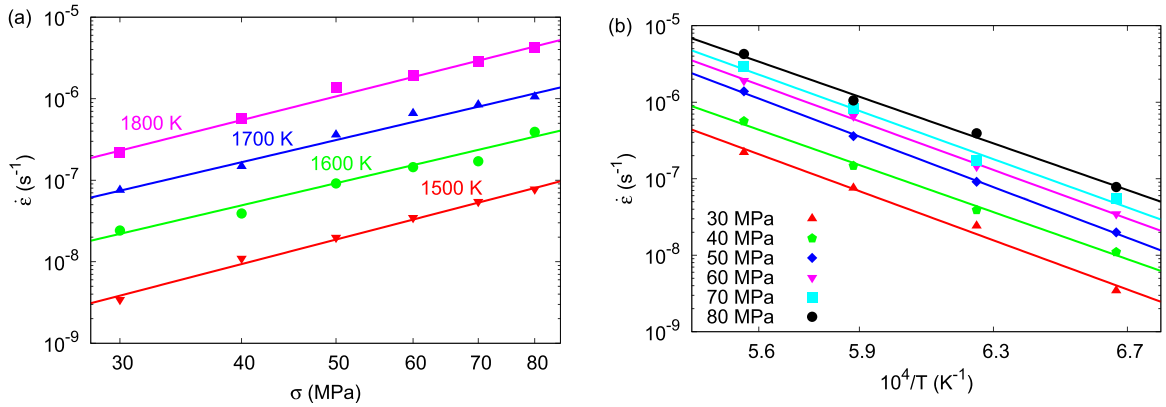

Fig. 6. (a) Creep strain rates as a function of applied creep stress σ for the different temperatures. (b) Variation of creep strain rates as a function of the reciprocal temperature T for all the applied stresses. Color lines represent the fitting of the data for (a) and (b). (For interpretation of the references to color in this figure legend, the reader is referred to the web version of this article).

Table 3
High temperature creep power law parameters obtained from experiments on MgO. SC and PC refer to single crystal and polycrystalline samples respectively.

Type of test	Sample	T Range (K)	n	Q (eV)	References
3-pt bend	SC	1723–1973	4.0–7.0	3.5–7.0	[43]
3-pt bend	SC	1573–1903	3.0	5.8	[44]
Compression	SC	1333–1773		4.8	[45]
Tension	SC	1473–1773	3.8 – 4.5	4.1	[46]
Compression	PC	1573–1733	3.2	3.3	[47]
Compression	PC	1473–1773	2.6	4.55, 4.81	[48]
Compression	PC	1473	3.3	2.21	[42]
Compression	SC	1573–1773	3.4	4.61	[35]
Compression	SC	1950–2000	3.0, 1.3		[49]
Compression	SC	1673–2073	4.2–8.5	3.6–4.4	[13]

plasticity of MgO. This allows us to do a step further and model creep conditions by including the climb mechanism in the same simulation framework. Creep results are usually described in term of a power law. The stress exponent is often considered as an indicator of the controlling mechanisms acting during creep deformation. In fact, diffusion creep results in a linear dependence between stress and strain rates, while dislocation creep is commonly identified by a stress exponent between 3 and 5. In this study, we observe a constant stress exponent close to 3 for the considered temperature and applied stress range. Several theoretical models predict the same exponent [41].

The value of creep activation enthalpy Q obtained from our calculations is 3.1 ± 0.2 eV, close to the oxygen self-diffusion enthalpy from Yoo et al. [30] – i.e. 3.24 eV – that we used as input parameter in Eq. (6) for all the simulations displayed in Fig. 6. Experimentally, it is recognized that for metals the activation energies of creep agree with the ones of self-diffusion of the slowest species [42], while for oxides and silicates such a correlation is not completely clear. Here we find the same agreement, demonstrating that climb is the limiting mechanism in high temperature creep. This is not surprising since the climb mobility is several orders of magnitude 10–13 depending on the considered creep stresses and temperatures) slower than the glide one.

A compilation of experimental values for n and Q [13,35,42–49] is provided in Table 3. First, it is worth pointing out that experimental conditions may vary substantially, making the comparison more difficult. Nevertheless, concerning the power law exponent, the values found in experiments generally agree with the ones proposed by predictive models. A deviation of n towards higher values is observed at lower temperatures [13,43]. In the latter case, this may be due to the presence of precipitates in some MgO samples, which would influence the creep behavior, while in the former case the deviation could be due to the fact that other extrinsic processes may become more important at lower temperatures, widening the variability range of n. These impurity-related interactions are not taken into account in our formulation, since it reproduces deformation in MgO single crystals where the role of impurities appears only through the point defect concentration introduced in the pre-exponential factor of the diffusion equation. Thus, in this study, the value of the power law exponents represents a lower limit of the predicted variability.

The activation enthalpy of creep gathered from experiments, on the other hand, often mirrors the one of oxygen self-diffusion in MgO. This is in agreement with our study. A slightly higher activation enthalpy in some cases is found and an interpretation of this difference is provided by Wolfenstine and Kohlstedt [35]. They propose that this energy difference could be due to jog formation enthalpy, which in climb-controlled creep may be an important factor, estimated at 1.2 eV. The remaining portion of creep activation enthalpy equals the one of oxygen self-diffusion, which agrees with the results reported in this study. In our formulation the jog formation energy is not included, since it is assumed that the dislocation lines are saturated with jogs. This provides an explanation of the difference we observe between our data and some experimental creep activation enthalpy values.

The influence of oxygen self-diffusion coefficients on strain rates is displayed in Fig. 8(a). The variability of four orders of magnitude between the extreme values of the diffusion coefficients [29] is reduced to three orders of magnitude of difference for the resulting creep strain rates.

To better compare our results with the experimental data on creep in MgO, another point of discussion must be addressed. The lowermost self-diffusion values obtained by Yang and Flynn [32] result from diffusion measurements performed on crystals having an exceptional degree of purity. These crystals do not show any significant impurity content and the surface damage contribution to diffusion is dramatically reduced. Such features contribute to lower the active impurity level during diffusion by a factor of ten below the one of high-quality commercial MgO [50]. Moreover, there is no evidence in the bibliography cited in Table 3 that the samples used in creep experiments were somehow resembling the ones of Yang and Flynn [32] in terms of crystal growing technique, impurity content and surface damage extent. Therefore, the latter samples are not considered representative with respect to the diffusion mechanism acting in the ones subjected to creep experiments. Considering as input parameters for self-diffusion those experimental results controlled by extrinsic oxygen diffusion [30,31] that better resemble the conditions at which natural crystals are subjected to creep, it is possible to focus on the upper half of the graph of Fig. 8(a) to draw a better comparison with experimental data. In these conditions, the strain rates obtained in this study bracket the experimental results for MgO, as can be viewed in Fig. 8(b).

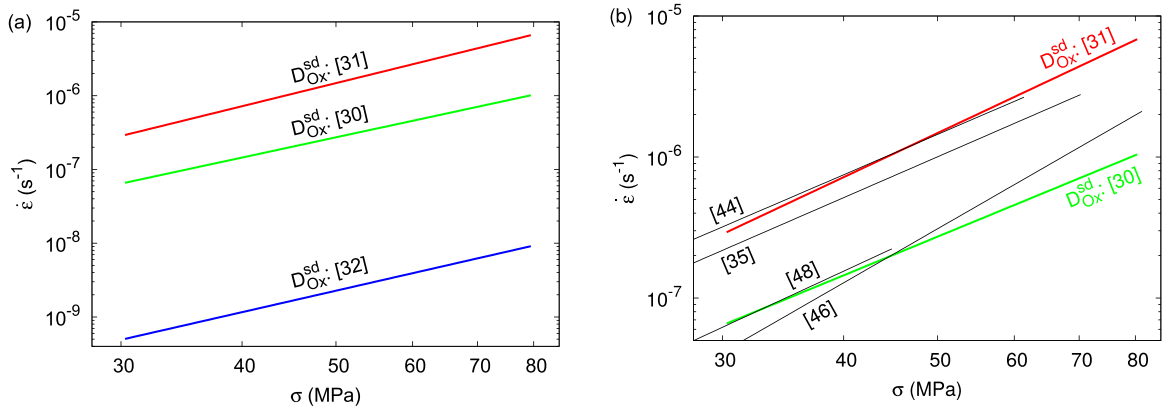

Fig. 8. Creep strain rates as a function of stress (color lines) at 1700 K using different oxygen self-diffusion coefficients as input parameters for the 2.5D-DD code (a) and their comparison with experimental data (black lines) (b). Numerical values for D^{sd}_{Ox} at 1700 K are provided in Table 2. (For interpretation of the references to color in this figure legend, the reader is referred to the web version of this article).

5. Conclusions

In the present work we applied a newly developed 2.5D-DD approach to MgO for the first time, in order to reproduce its deformation under three different temperature regimes. At low and intermediate temperatures our results agree with previous numerical (3D-DD) and experimental evidences, providing a benchmark on the validity of our approach. This allowed us to do a step further and introduce dislocation climb at high temperatures, where this mechanism has a relevant role on creep of MgO crystals. This was not feasible in previous 3D-DD formulations, due to the computational complexity of coupling phenomena occurring on very different time scales (such as dislocation glide and climb). Results in this regime mirror the available experimental data on high temperature creep of MgO, confirming that the present numerical tool is capable of reproducing the plastic behavior of this phase under varying conditions and driving mechanisms.

Acknowledgment

Financial support by the European Research Council under the Seventh Framework Program (FP7), ERC Grant no. 290424 Rheoman, is gratefully acknowledged. Computational resources have been provided by the CRI-Université de Lille 1.

References

[1] J. Amodeo, P. Carrez, B. Devincre, P. Cordier, Multiscale modelling of MgO plasticity, Acta Mater. 59 (2011) 2291–2301. http://dx.doi.org/10.1016/j.actamat.2010.12.020.
[2] J. Amodeo, P. Carrez, P. Cordier, Modelling the effect of pressure on the critical shear stress of MgO single crystals, Philos. Mag. 92 (2012) 1523–1541. http://dx.doi.org/10.1080/14786435.2011.652689.
[3] J. Amodeo, S. Dancette, L. Delannay, Atomistically-informed crystal plasticity in MgO polycrystals under pressure, Int. J. Plast. 82 (2016) 177–191. http://dx.doi.org/10.1016/j.ijplas.2016.03.004.
[4] J.P. Hirth, J. Lothe, Theory of Dislocations, Wiley, 1992.
[5] A. Arsenlis, W. Cai, M. Tang, M. Rhee, T. Oppelstrup, G. Hommes, T.G. Pierce, V.V. Bulatov, Enabling strain hardening simulations with dislocation dynamics, Model. Simul. Mater. Sci. Eng. 15 (2007) 553–595. http://dx.doi.org/10.1088/0965-0393/15/6/001.
[6] L.P. Kubin, G. Canova, M. Condat, B. Devincre, V. Pontikis, Y. Bréchet, Dislocation microstructures and plastic flow: a 3D simulation, Solid State Phenom. 23–24 (1992) 455–472. http://dx.doi.org/10.4028/www.scientific.net/SSP.23-24.455.
[7] D. Gómez-García, B. Devincre, L.P. Kubin, Forest hardening and boundary conditions in 2-D simulations of dislocation dynamics, MRS Proc. 578 (1999) 131. http://dx.doi.org/10.1557/PROC-578-131.
[8] D. Gómez-García, B. Devincre, L.P. Kubin, Dislocation patterns and the similitude principle: 2.5D mesoscale simulations, Phys. Rev. Lett. 96 (2006) 8–11. http://dx.doi.org/10.1103/PhysRevLett.96.125503.
[9] A. Benzerga, Y. Bréchet, A. Needleman, E. Van Der Giessen, Incorporating three-dimensional mechanisms into two-dimensional dislocation dynamics, Model. Simul. Mater. Sci. Eng. 12 (2004) 557–559. http://dx.doi.org/10.1088/0965-0393/12/3/C01.
[10] K.M. Davoudi, L. Nicola, J.J. Vlassak, Dislocation climb in two-dimensional discrete dislocation dynamics, J. Appl. Phys. 111 (2012). http://dx.doi.org/10.1063/1.4718432.
[11] S.M. Keralavarma, T. Cagin, A. Arsenlis, A.A. Benzerga, Power-law creep from discrete dislocation dynamics, Phys. Rev. Lett. 109 (2012) 1–5. http://dx.doi.org/10.1103/PhysRevLett.109.265504.
[12] F. Boioli, P. Carrez, P. Cordier, B. Devincre, M. Marquille, Modeling the creep properties of olivine by 2.5-dimensional dislocation dynamics simulations, Phys. Rev. B 92 (2015) 014115. http://dx.doi.org/10.1103/PhysRevB.92.014115.
[13] J.L. Routbort, Work hardening and creep of MgO, Acta Metall. 27 (1979) 649–661.
[14] P. Carrez, P. Cordier, B. Devincre, L.P. Kubin, Dislocation reactions and junctions in MgO, Mater. Sci. Eng. A 400–401 (2005) 325–328. http://dx.doi.org/10.1016/j.msea.2005.03.071.
[15] B. Karki, R. Wentzcovitch, S. de Gironcoli, S. Baroni, High-pressure lattice dynamics and thermoelasticity of MgO, Phys. Rev. B 61 (2000) 8793–8800. http://dx.doi.org/10.1103/PhysRevB.61.8793.
[16] J. Amodeo, B. Devincre, P. Carrez, P. Cordier, Dislocation reactions, plastic anisotropy and forest strengthening in MgO at high temperature, Mech. Mater. 71 (2014) 62–73. http://dx.doi.org/10.1016/j.mechmat.2014.01.001.
[17] U. Kocks, A. Argon, M. Ashby, B. Chalmers, J. Christian, T. Massalski, Progress in Material Science, Pergamon, 1975.
[18] F. Appel, B. Wielke, Low temperature deformation of impure MgO single crystals, Mater. Sci. Eng. 73 (1985) 97–103. http://dx.doi.org/10.1016/0025-5416(85)90299-X.
[19] C. Barthel, (Ph.D. thesis), University of Gottingen, 1984.
[20] F. Sato, K. Sumino, The yield strength and dynamic behaviour of dislocations in MgO crystals at high temperatures, J. Mater. Chem. 15 (1980) 1625–1634.
[21] M. Srinivasan, T.G. Stoebe, Temperature dependence of yielding and work-hardening rates in magnesium oxide single crystals, J. Mater. Sci. 9 (1974) 121–128. http://dx.doi.org/10.1007/BF00554762.
[22] C. Hulse, J. Pask, Mechanical properties of magnesia single crystals in corn pression, J. Am. Ceram. Soc. 43 (1960) 373–378. http://dx.doi.org/10.1177/058310248001200917.
[23] L.P. Kubin, Dislocations, Mesoscale Simulations and Plastic Flow 5, Oxford University Press, 2013.
[24] R. Madec, B. Devincre, L.P. Kubin, From dislocation junctions to forest hardening, Phys. Rev. Lett. 89 (2002) 255508. http://dx.doi.org/10.1103/PhysRevLett.89.255508.
[25] B. Devincre, L. Kubin, T. Hoc, Physical analyses of crystal plasticity by DD simulations, Scr. Mater. 54 (2006) 741–746. http://dx.doi.org/10.1016/j.scriptamat.2005.10.066.
[26] L.M. Hirsch, T.J. Shankland, Equilibrium point defect concentrations in MgO: understanding the mechanisms of conduction and diffusion and the role of Fe impurities, J. Geophys. Res. 96 (1991) 385–403. http://dx.doi.org/10.1029/90JB02175.
[27] D. Alfè, M. Gillan, Schottky defect formation energy in MgO calculated by diffusion Monte Carlo, Phys. Rev. B – Condens. Matter Mater. Phys. 71 (2005). http://dx.doi.org/10.1103/PhysRevB.71.220101.
[28] K. Ando, Y. Kurokawa, Y. Oishi, Oxygen self-diffusion in Fe-doped MgO single crystals, J. Chem. Phys. 78 (1983) 6890–6892. http://dx.doi.org/10.1063/1.444635.
[29] J. Van Orman, K. Crispin, Diffusion in oxides, Rev. Mineral. Geochem. 72 (2010) 757–825. http://dx.doi.org/10.2109/jcersj1950.74.851_215.
[30] H. Yoo, B.J. Wuensch, W.T. Petuskey, Oxygen self-diffusion in single-crystal MgO: secondary-ion mass spectrometric analysis with comparison of results from gas – solid and solid – solid exchange, Solid State Ion. 150 (2002) 207–221.
[31] Y. Oishi, W.D. Kingery, Oxygen diffusion in periclase crystals, J. Chem. Phys. 33 (1960) 905–906. http://dx.doi.org/10.1063/1.1731286.
[32] M. Yang, C. Flynn, Intrinsic diffusion properties of an oxide: MgO, Phys. Rev. Lett. 73 (1994) 1809–1812.
[33] D. Caillard, J.L. Martin, Thermally Activated Mechanisms in Crystal Plasticity 8, Elsevier, 2003.
[34] F. Boioli, A. Tommasi, P. Cordier, S. Demouchy, A. Mussi, Low steady-state stresses in the cold lithospheric mantle inferred from dislocation dynamics models of dislocation creep in olivine, Earth Planet. Sci. Lett. 432 (2015) 232–242. http://dx.doi.org/10.1016/j.epsl.2015.10.012.
[35] J. Wolfenstine, D.L. Kohlstedt, Creep of (Mg,Fe)O single crystals, J. Mater. Sci. 23 (1988) 3550–3557. http://dx.doi.org/10.1007/BF00540494.
[36] S.J. Basinski, Z.S. Basinski, Plastic deformation and work hardening, Dislocations Solids 4 (1980) 261–362.
[37] J. Durinck, B. Devincre, L. Kubin, P. Cordier, Modeling the plastic deformation of olivine by dislocation dynamics simulations, Am. Mineral. 92 (2007) 1346–1357. http://dx.doi.org/10.2138/am.2007.2512.
[38] J. Girard, G. Amulele, R. Farla, A. Mohiuddin, S.I. Karato, Shear deformation of bridgmanite and magnesiowüstite aggregates at lower mantle conditions, Science 351 (2016) 144–147. http://dx.doi.org/10.1126/science.aad3113.
[39] A. Kraych, P. Carrez, P. Hirel, E. Clouet, P. Cordier, Peierls potential and kink-pair mechanism in high-pressure $MgSiO_3$ perovskite: an atomic scale study, Phys. Rev. B – Condens. Matter Mater. Phys. 93 (2016) 1–9. http://dx.doi.org/10.1103/PhysRevB.93.014103.
[40] S. Ritterbex, P. Carrez, K. Gouriet, P. Cordier, Modeling dislocation glide in Mg2SiO4 ringwoodite: towards rheology under transition zone conditions, Phys. Earth Planet. Inter. 248 (2015) 20–29. http://dx.doi.org/10.1016/j.pepi.2015.09.001.
[41] J. Weertman, Theory of steady-state creep based on dislocation climb, J. Appl. Phys. 26 (1955) 1213–1217. http://dx.doi.org/10.1063/1.1721875.
[42] T. Langdon, J. Pask, The mechanism of creep in polycrystalline magnesium oxide, Acta Mater. 18 (1970) 505–510.
[43] R.L. Cummerow, High-temperature steady-state creep rate in single-crystal MgO, J. Appl. Phys. 34 (1963) 1724. http://dx.doi.org/10.1063/1.1702668.
[44] W.S. Rothwell, A.S. Neiman, Creep in vacuum of MgO single crystals and the electric field effect, J. Appl. Phys. 36 (1965) 2309. http://dx.doi.org/10.1063/1.1714469.
[45] A.G. Atkins, D. Tabor, Mutual indentation hardness of single-crystal magnesium oxide at high temperatures, J. Am. Ceram. Soc. 2412 (1967) 195–198.
[46] A. Clauer, B. Wilcox, High temperature tensile creep of magnesium oxide single crystals, J. Am. Ceram. Soc. 59 (1976) 89–96.
[47] J.B. Bilde-Sorensen, Dislocation structures in creep-deformed polycrystalline MgO, J. Am. Ceram. Soc. 55 (1972) 606–610.
[48] J. Hensler, G. Cullen, Stress, temperature, and strain rate in creep of magnesium oxide, J. Am. Ceram. Soc. 51 (1968) 557–559.
[49] K.S. Ramesh, E. Yasuda, S. Kimura, Negative creep and recovery during high-temperature creep of MgO single crystals at low stresses, J. Mater. Sci. 21 (1986) 3147–3152. http://dx.doi.org/10.1007/BF00553350.
[50] M.H. Yang, C.P. Flynn, Ca^{2+} and $^{18}O^{2-}$ diffusion in ultrapure MgO, J. Phys. Condens. Matter 8 (1996) L279–L283. http://dx.doi.org/10.1088/0953-8984/8/18/001.